



Rock Porous Structure Characterization: A Critical Assessment of Various State-of-the-Art Techniques

Mehdi Razavifar, et al. [full author details at the end of the article]

Received: 25 March 2020 / Accepted: 20 November 2020 / Published online: 3 January 2021
© Springer Nature B.V. 2021

Abstract

The porous structure of geomaterials is of utmost importance for various industrial and natural processes. In this study, various conventional porous structure characterization techniques such as mercury intrusion porosimetry (MIP), nuclear magnetic resonance (NMR), micro-X-ray computed tomography (μ CT) imaging, as well as gas injection have been employed to perform a systematic and critical evaluation of all such techniques for characterization of a carbonate rock sample porous structure. The porosity obtained from μ CT (5 μ m/voxel) (21.5%) is closer than the overall porosity obtained by MIP (17.23%) to the gas porosimetry result (23%). The 5% difference could be due to inaccessible pores to mercury, which can be accessible to nitrogen with much smaller molecules. The porosity obtained from NMR is 21.4%. It is lower than porosity values by μ CT (5 μ m/voxel) and by gas injection and higher than the prediction of MIP. The porosity is obtained by μ CT, but the much lower resolution (27.5 μ m/voxel) results in 8.19% underestimating the porosity by around 50%. Regarding permeability, the results of the NMR technique are highly dependent on the cutoff range used and very different from other techniques, whereas the permeability obtained by MIP is around 18.42 mD, close to that obtained by gas permeameter (20 mD). The μ CT imaging provides the opportunity to measure pore and throat size distribution directly, to achieve open and closed porosity, the coordination number of pores and surface and volume characteristics of the porous medium, which can hardly be performed through other techniques. The resolution of images, however, fully controls the obtained pore and throat size distribution in CT analysis. The Kolmogorov–Smirnov distribution analysis reveals that the resulting pore size distribution from MIP is rather a rough estimation of the throat size distribution obtained from μ CT (5 μ m/voxel), while NMR prediction can provide a rather good approximation of the pore size distribution obtained from μ CT (5 μ m/voxel). The NMR prediction is however dependent on the choice made for the surface relaxivity coefficient, and changing it would significantly affect the resulting distribution. The results of this study provide further insight and elucidate the differences of the quantities such as porosity, permeability, and pore and throat size distribution obtained from various techniques which are essential either as an input to numerical models of flow and transport in porous media or as a building block of the theoretical models.

Keywords NMR · Micro-CT scan · MIP · Pore size distribution · Porosity · Pore throat distribution

Abbreviations

BVI Bulk volume irreducible

CPMG	Carr–Purcell–Meiboom–Gill
CT	Computed tomography
FFI	Free fluids index
GIT	Green imaging technologies
MIP	Mercury intrusion porosimetry
NMR	Nuclear magnetic resonance
PSD	Pore size distribution
SNR	Signal-to-noise ratio
XRD	X-ray diffractometer
PDP	Pulse-decay permeametry
ROI	Region of interest
SEM	Scanning electron microscopy
FIB–SEM	Focused ion beam–scanning electron microscopy
HIM	Helium ion microscopy
CDF	Cumulative distribution function
GIW	Generalized inverse Weibull distribution

SI unit

Pressure	1 psi (6894.76 Pa)
Permeability	1 mD (0.9869 μm^2)

1 Introduction

The structure of a porous medium affects its physical, chemical, and mechanical properties. Therefore, the characterization of porous media is crucial for monitoring and modeling many natural and industrial processes. In oil recovery, for instance, a reasonable estimation of the recovery factor would not be possible without an in-depth understanding of reservoir production mechanisms and a proper evaluation of reservoir rock porous structure. In shale gas exploitation (Gao et al. 2018; Klaver et al. 2015; Ma et al. 2019; Qiu et al. 2020, 2019a, b; Tan et al. 2019; Zhang et al. 2019; Zhao et al. 2019), coalbed methane production (Li et al. 2018, 2017; Song et al. 2019; Zhang et al. 2018; Zhao et al. 2017), and carbon sequestration (Adebayo et al. 2017; Dejam and Hassanzadeh 2018a, b), knowledge of porous structure and pore connectivity is essential for studying fluid storage and transport properties. On the other hand, mechanical properties, such as the compressive strength of porous cementitious materials, are controlled by porosity and pore size distribution (Hou et al. 2019). Furthermore, pore connectivity and porous structure are key factors controlling the migration of contaminations in soils, as well as moisture transport in bricks and wood. It is, therefore, obvious that the more precise the characterization methods of porous media are, the more accurate modeling resulting in various phenomena of interest in industrial and natural porous media would be.

For porous media characterization, several methods have been established, such as gas injection, mercury intrusion porosimetry (MIP), nuclear magnetic resonance (NMR), and computed tomography and micro-computed tomography (μCT) (Spanne et al. 1994; Benavides et al. 2020; Ghomeshi et al. 2018).

While these three techniques are most widely used as common practice in porous media characterization, there has been a wealth of new techniques which in recent years have been introduced. The μCT is applicable for capturing mm- to μm -scale features, for instance,

sedimentary laminations and micro-fractures. In order to enter the realm of nanometer parts of the porous skeleton, focused ion beam–scanning electron microscopy (FIB–SEM) for visualizing pores of tens to hundreds nm and focused ion beam–helium ion microscopy (FIB–HIM), providing the possibility of capturing sub-10 nm pores, have been developed and employed (Wu et al. 2020). However, FIB–SEM and FIB–HIM result in 2D images, while μ CT can capture three-dimensional images. Introduced first in biological sciences, laser confocal microscopy provides the opportunity to obtain 3D images of porous media with high resolution (submicron, hundreds of nm) nondestructively. Laser confocal microscopy application is, however, limited by its laser penetration depth in the solids (Fredrich 1999).

The need to extract further data from mere 2D slices of the porous skeleton and to obtain a full 3D depiction of porous media based on the basic data such as grain size distribution has resulted in the development of 3D reconstruction techniques (Adler et al. 1990; Thov-ert et al. 1993; Thovert et al. 2001; Øren and Bakke 2002; Hidajat et al. 2002, Mourzenko et al. 2011; Tinet et al. 2020). In addition to the statistical techniques such as two-point and multiple-point statistics, researchers have also examined the use of synthetically generated porous media images by means of fractals and cellular automata (Hernández Zubeldia et al. 2016), which have the potential to produce complex objects based on the simple mathematical rules. The difficulty which these porous media reconstruction techniques face is the selection of suitable criteria assuring the similarity of the produced object with the natural one and achieving the same level of connectivity as the target porous skeleton. The simulation of flow inside either the reconstructed porous media (e.g., Adler et al. 1990) or on the images obtained by CT imaging (Mostaghimi et al. 2013) has also been employed to shed light into the transport properties of porous media. For this purpose, different approaches such as Stokes flow directly solved on binarized three-dimensional rock images (Mostaghimi et al. 2013) or single- and two-phase flow simulations based on the invasion percolation theory or critical point theory applied in the extracted pore networks (Ghared-aghloo et al. 2018; Franc et al. 2020) are used. Other noticeable progress recently made in the porous media characterization is the use of nanoparticle tracking to probe porous media and sense its transport characteristics (Wu and Schwartz 2020), the use of machine learning and deep learning to link pore morphology to permeability (Kamrava et al. 2020), and the learning from 2D X-ray images and predicting the porous media characteristics such as porosity, surface area and average pore size (Alqahtani et al. 2020). Finally, the use of Minkowski functionals for porous media characterization (Armstrong et al. 2019) gives a more refined description of the porous medium characteristics including its connectivity and can therefore be better linked to macroscale porous media properties.

Despite such remarkable progress made in different numerical and experimental techniques in porous media characterization, there are only few studies in the literature which address the differences and similarities in the result of different techniques such as MIP, NMR, and μ CT and rarely compare all such techniques and their scope of application, particularly for reservoir rocks. Furthermore, these state-of-the-art techniques suffer from technical limitations and shortcomings in the conceptual models commonly used to interpret their results. For instance, even though the porous structure is made of two distinct elements, namely pores and throats, some of these methods fail to distinguish pores and throats. While pores are having much more volume of their own as compared to the throats, thereby controlling the storage of fluids, throats mainly control the connectivity and transmissibility of porous media.

Washburn was one of the first to introduce a method for porous media characterization (Washburn 1921). This method, nowadays known as MIP, is based on a bundle of

capillary tubes model that is not analogous to a network of pores and throats, which constitutes a real porous structure. Having failed to distinguish between these two distinct functions of pores and throats, the bundle of the capillary tube model is unable to portray porous soil structure and its characteristics correctly. That is why some researchers have referred to the distribution of voids obtained from MIP as pore access size distribution (Feia et al. 2014). In fact, it is neither pore size nor throat size distribution.

Moreover, as NMR analysis can sense the responses of hydrogen atoms in both throats and pores, its results could also be representative of both distributions. The results obtained from these measurements are often employed either to predict porous media characteristics such as permeability and capillary pressure–saturation curves or to analyze the changes of the porous structure under environmental loads such as temperature change or stress (Gao et al. 2019). The question is, therefore, if one can directly find the pore and throat size distribution from imaging methods such as μ CT imaging, how the distributions obtained from NMR and MIP correlate to such data. Are they different? To which extent? The current literature lacks the answer to such questions.

Song et al. (2019) employed scanning electron microscopy images and NMR imaging to obtain coal permeability and pore size distribution. The pore size distribution obtained from NMR and that of SEM were found to be similar. In their SEM image processing, however, all voids were considered as pores. It is, moreover, noteworthy that SEM analysis is unable to capture the actual three-dimensional morphology and shape of pores and throats.

Wang et al. (2020) compared the pore size distribution of coal samples obtained by MIP and μ CT analysis. There was no division of porous space of coal matrix to pores and throats; they instead considered pores of coal matrix, solely, and the fracture network of the coal sample. The volumetric fraction of pores measured using MIP at the nanometer-scale (0.2–1 μ m diameter) was much higher than the one obtained using μ CT image analysis. The volumetric fraction of pores at the micrometer-scale (1–40 μ m diameter) measured by MIP was much lower than the contribution measured using μ CT image analysis. The largest volumetric contribution was found for the pores in 1–10 μ m diameter when measured using MIP. The μ CT image analysis resulted in the largest volumetric contribution for the pores in a 10–20 μ m diameter range. The complex nature of the porous coal matrix could limit the application of their findings to other rock types. Furthermore, their study does not include the results of NMR analysis.

This brief review highlights the need to compare porous media characteristics obtained by MIP, μ CT, as well as NMR altogether and to distinguish between pores and throats in the analysis, which has been overlooked in the previous studies.

Thus, in order to address the mentioned shortcomings of the current literature, we have applied four state-of-the-art techniques with a wide range of detected pores, namely gas injection (helium porosimetry), MIP, NMR, and μ CT (Fig. 1) on a certain rock sample, and then, their results have been thoroughly investigated.

We intend to address the following issues:

- (a) Can we obtain pore and throat size distribution from different methods?
- (b) What are the limitations and scope of application of each technique?
- (c) How different are the results of various methods?
- (d) What are the deficiencies in models used for interpreting the results in terms of pore size distribution?

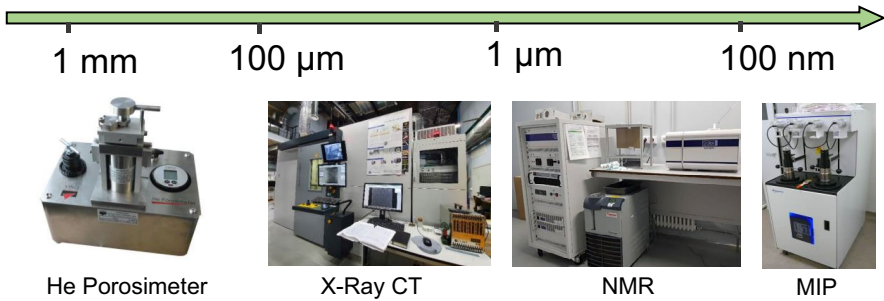


Fig. 1 The set of experimental techniques with a highlighted range of measured pore size

- (e) Which method is suitable for which process and type of analysis (i.e., transport, storage, ...)?

It is noteworthy that the target (carbonate) rock is characterized by a wide range of pores from nano- to macrosizes. In order to process the global structure of the sample, one should start at low-resolution or bulk measurements by scanning the full sample size. The next steps require detailed investigation at a higher resolution. The experimental workflow is of high importance for complex objects such as carbonates. For instance, the image resolution is a crucial parameter in X-ray CT analysis of the rock; therefore, the resolution of the scanning should prevail the characteristic size of the pore. For this reason, the analysis of μ CT is performed at two resolutions to inspect the influence of imaging resolution on the results.

In this study, we summarize the results of the experimental investigation of the core sample by a suite of state-of-the-art techniques, including CT and μ CT, NMR, and MIP. Analysis of our findings results in the discussion on the advantages and limitations of each method. In Sect. 2, we introduce the sample characteristics and provide details on experimental techniques. Section 3 outlines the obtained results from various porous media characterization techniques, and a comparison of the results highlights the scope of application and merits and demerits of each. It is followed by the summary and conclusions in Sect. 4.

2 Materials and Methods

2.1 Rock Samples and Rock Composition

The rock samples used in this study are outcrops and were taken from Iran. An X-ray diffractometer (D8 Advance, Bruker, Germany) was employed to inspect the structure of the rock samples. Results of XRD analysis revealed that the dominant mineral of the rock sample is dolomite ($\text{CaMg}(\text{CO}_3)_2$). Figure 2 illustrates the applied workflow of core investigation.

2.2 Porosity and Permeability Measurement

Gas expansion porosimeter and permeameter (VINCI, France) were utilized to measure the porosity and permeability of the core plugs. The gas expansion porosimeter determines

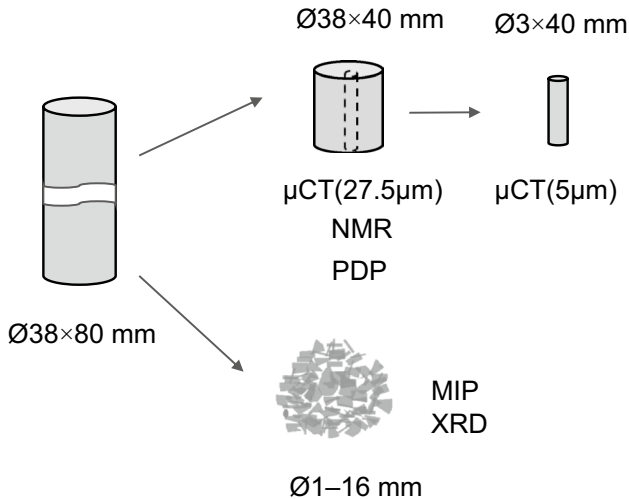


Fig. 2 The workflow of core sample investigation

the porosity of the core plugs based on Boyle's law for gases. It could measure up to 60% porosity. The gas permeameter (PDP) was capable of measuring permeability in the range of 0.5 mD to 5 D. Nitrogen was used as the gas for these measurements.

2.3 Porous Structure Characterization

Various state-of-the-art methods were employed to get insight into the pore and pore throat size distributions of the rock samples. The methods include X-ray Micro-Computed Tomography (μCT) and Nuclear Magnetic Resonance (NMR), as well as Mercury Intrusion Porosimetry (MIP). In order to perform a CT scan, an X-ray system for Computed Tomography (Phoenix vltomelx L240/180 by GE Sensing & Inspection Technologies GmbH) was used. The nano-focus X-ray tube was utilized for μCT scan analysis. The analysis of the 3D image was performed on the Math2Market GeoDict software package. NMR analysis was performed by Geospec 2/53 low-field relaxometer (Oxford Instruments Inc.). Its procedure is detailed in the subsequent section. Mercury Intrusion Porosimetry was performed by means of Auto Pore IV 9500 unit (Micrometrics). The analysis was performed with a high-pressure model, which could sense pore diameter as small as $0.003 \mu\text{m}$.

2.3.1 MIP Experimental Procedure

A Micrometrics Autopore IV 9500 Porosimeter was used to precisely measure the amount of mercury being injected into the rock sample. After weighting the cleaned and dried rock sample, a proper penetrometer was selected, and the sample was placed inside the rig. Then, the assembly was loaded into the low-pressure chamber of the apparatus. The penetrometer was evacuated to a pressure of less than 0.0009 psia, and filled with mercury at a pressure of 0.5 psia. The bulk volume of the sample was determined at this point. The injection pressure of mercury into the rock sample increased incrementally from 0.5 to 30 psia. After equilibrium was established in the last step (i.e., 30 psia), injection pressure was

reduced to the atmospheric pressure, and the penetrometer was removed. The penetrometer was then loaded into the high-pressure chamber of the Autopore system. The mercury was injected into the core plug at increasing incremental pressures (up to 60,000 psia). At each pressure point, mercury intrusion was monitored, while the pressure was held constant. Equilibrium was identified when the rate of intrusion dropped below 0.001 $\mu\text{L/g-sec}$. Finally, mercury saturations were calculated as a percentage of the pore volume at each pressure. The pore volume used for calculation of mercury saturation was obtained from the maximum intrusion volume of mercury. In the following, the procedure for the determination of pore size distribution by means of MIP experiments is described (Rezaei et al. 2020):

Firstly, a graph of the fraction of pore volume injected (v) versus pore access radius (r) can be constructed, and the differential of this gives a pore throat size distribution (PSD) function:

$$\text{PSD} = \frac{dv}{d \log(r)} \quad (1)$$

The differential is calculated numerically. The central difference method is used to calculate PSD as:

$$\text{PSD}_i = \frac{v_{i+1} - v_{i-1}}{\log(r_{i+1}) - \log(r_{i-1})} \quad (2)$$

Then, PSD is smoothed as:

$$\text{PSD}_i = \frac{\text{PSD}_{i-1} + 2\text{PSD}_i + \text{PSD}_{i+1}}{4} \quad (3)$$

PSD is then normalized to 1 as follows:

$$\text{PSD}_{\text{normal}i} = \frac{\text{PSD}_i}{\text{PSD}_{\text{max}}} \quad (4)$$

and finally, the normalized PSD is presented in the graphical form. Furthermore, based on the mercury capillary pressure–saturation curves and Laplace equation, one can obtain volume fraction–size distributions. The size of corresponding pores (r), idealized as capillary tubes, is obtained from Laplace equation and the saturation change provides the volume fraction of the associated pores. The standard Laplace's law, in which γ is the surface tension and θ is the contact angle, reads as follows:

$$P = \frac{2\gamma \cos \theta}{r} \quad (5)$$

2.3.2 Experimental Procedure and Setting for μCT

In recent decades, there has been a growing appeal in the use of CT imaging in the oil and gas industry. Tomography gives a three-dimensional image of the rock sample (Cnudde and Boone 2013). Current improvements in scan quality resolution, with enhanced voxel size in the range of micrometers, usually referred to as μCT to emphasize on the resolution as well as developments in specialized software for 3D image processing, allow extracting most important structural parameters of the samples. These parameters can then be used to

estimate other macroscale physical characteristics of the samples such as permeability, diffusivity, and sweep efficiency, eventually information required for the development of oil and gas fields (Remeysen and Swennen 2008).

The X-ray CT system is equipped with two X-ray tubes. The micro-focused, higher power tube is usually used for large objects and dense materials as capable of working at higher energy (accelerating voltage) and power (up to 320 W). For geological samples, this usually refers to cores with a diameter of 30 mm and higher. The nano-focused one with a tunable size of the focal spot to less than 1 μm and capable for tomography with voxel size 1 μm and even less is a choice for a high-resolution μCT and usually applied for samples with diameter less than 30 mm. The detector is a 2024×2024 photodiode array with a scintillator and 400 by 400 mm size. For this system, the highest resolution or minimal voxel size for a full sample width would be around 1/2000 of its size and hence a function of sample size: for example, with a core diameter of 100 mm, a voxel is down to 50 μm , for core 8 mm diameter—4 μm . The original core was investigated at voxel size 27.5 μm and 8 mm mini core drilled out of it at a voxel size of 5 μm .

2.3.3 Extraction of Pore and Throat Size Distribution from μCT Images

The analysis of pore size distribution was performed using the GeoDict software (Math2Market) with two techniques: granulometry and porosimetry modes for analysis of the size of pores and throats between open ones. Additionally, a mercury intrusion porosimetry (MIP) simulation could be performed, which provides a simulated relationship between applied pressure and invaded volume to determine the radius of the pores accessible by the mercury. Therefore, the obtained pore size distribution does not include all pores but solely the ones connected to the boundaries. The cylindrical pore geometry assumption and the bundle of capillary tube conceptualization are two significant problems associated with MIP (both in experimental and simulation approaches). The bundle of capillary tube conceptualization has this shortcoming that the large pores behind small necks are considered small pores. This leads to an overestimation of the number of small pores and an underestimation of large pores (Moro and Böhni 2002). Erosion and dilation of the pore space are employed in GeoDict to simulate MIP, morphologically. The pore space is eroded with a sphere of a certain radius, then the part disconnected from the boundaries is removed, and the remaining part dilated again. Through this process, one would obtain the pore space that is reached by a sphere of radius R_{MIP} flowing in from the boundary (Büttner 2011; Wiegmann 2007). The same procedure has been utilized by Hilpert and Miller (2001), Arns et al. (2005), and Sweijen et al. (2017). The geometrical pore size distribution includes all pores and is based on the size of the spheres placed into the pores. The detailed procedure of these two techniques can be found in the literature (Büttner 2011; Kim et al. 2013).

2.3.4 Experimental Procedure and Setting for NMR Core Analysis

Low-field NMR relaxometry was used as one of the methods for porous structure analysis. All experiments were performed on a Geospec 2/53 relaxometer (Oxford Instruments Inc.). The NMR relaxometer used in the core plugs specifications study is a laboratory analyzer of core material operating at 2.28 MHz frequency with a magnetic field of 0.05 T.

NMR relaxometer is designed to measure the NMR T_1 and T_2 relaxation times (spin–lattice and spin–spin relaxation) in rock samples of cylindrical shape (core plugs) with a diameter of up to 53 mm. The principle of NMR operation is based on absorption by

the substance of electromagnetic energy caused by the magnetic moments of atomic nuclei (in our case, hydrogen) reorientation.

In this study, an NMR setup with a set of preset gradient coils located along each side of the magnet was used. These coils make it possible to additionally determine the saturation of samples with hydrogen-containing liquids, as well as to measure the time of transverse relaxation along the selected core axis—the one-dimensional saturation profile and the spatial T_2 spectrum. The obtained data is processed using Green Imaging Technologies (GIT) Systems Advanced v.7.5.1 software. The proposed scheme of investigations is presented in Fig. 3.

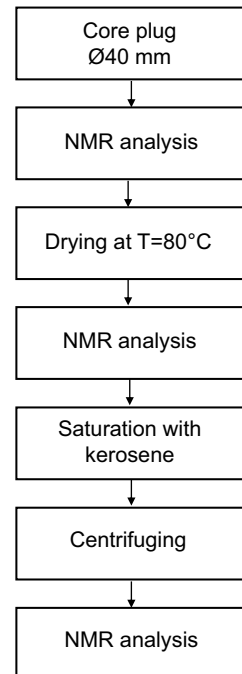
After sample preparation, NMR measurements were performed with the determination of the following parameters:

- The volume of NMR fluid according to T_2 test and total porosity;
- Saturation profile along the sample axis to ensure the 100% saturation of the core plug;

T_2 relaxation curves were measured by the Carr–Purcell–Meiboom–Gill method (CPMG); the time echo ($TE=2\tau$) was set to 0.1 ms. The number of trains (accumulations) of the pulse sequence ($90^\circ - \tau - 180^\circ - 2\tau - 180^\circ - \dots - 180^\circ$) was selected based on the results of the performed demo test on the core plug and estimated the highest signal-to-noise ratio (SNR).

The results of NMR measurements were analyzed based on general principles and interpretation schemes used by NMR specialists in the petrophysical industry (Abragam and Abragam 1961; Bloembergen et al. 1948; Callaghan 1993; Morriss et al. 1997). The sample porosity is calculated by T_2 results for a fully saturated sample. After testing the samples in the as-received state, samples were being dried at $T=80^\circ\text{C}$ in an oven for

Fig. 3 The proposed scheme of NMR investigations



48 h. Then, the NMR analysis was repeated. Samples were saturated with kerosene. The samples' saturation was performed using an automated core saturator at the pressure up to 120 bar with a duration not less than 48 h. Saturated samples were carefully prepared for further NMR testing and measured on X-ray Computed Tomography. After NMR on the saturated core was complete, both samples were sent for centrifuging in order to model the irreducible saturation state. Samples with 100% kerosene saturation and irreducible saturation were repeatedly delivered for the next step of NMR analyses.

There are two main approaches to an approximate permeability assessment based on T_2 relaxation time—the Timur–Coates (Timur 1968) and the Schlumberger–Doll Research (Bryant et al. 1993; Morriss et al. 1997) models. In our study, we have estimated the permeability of the sample utilizing the cutoff and spectral mode of Coates model:

$$K_{coates} = \left[\left(\frac{\varphi}{C} \right) \frac{MFFI}{MBVI} \right]^2 \quad (6)$$

where φ is the effective NMR porosity, MFFI and MBVI are the number of free and bound fluids in the sample determined after centrifuging the sample; C is a numerical coefficient.

The pore size distribution is calculated from the results of T_2 relaxation times. The relaxation time T_2 is described by the following expressions:

$$\frac{1}{T_2} = \frac{1}{T_{2b}} + \frac{1}{T_{2s}} + \frac{1}{T_{2d}}, \quad \text{where } \frac{1}{T_{2s}} = \rho \left(\frac{S}{V} \right)_{\text{pore}} \quad (7)$$

where T_2 is the transverse relaxation time of the pore fluid measured by the CPMG cycle; T_{2b} is the relaxation time T_2 of the pore fluid; T_{2s} is the pore fluid relaxation time T_2 associated with surface relaxation; T_{2d} is the relaxation time of the pore fluid caused by diffusion in a gradient magnetic field; ρ is the relaxation activity of the rock (T_2 relaxation force on grain surfaces); $(S/V)_{\text{pore}}$ is the ratio of pore surface area to pore volume (specific surface).

In the calculation of the pore size distribution, the surface relaxivity coefficient (ρ) is a crucial parameter. This coefficient mainly depends on rock properties and, therefore, is difficult to be obtained experimentally. The existing methods for defining the surface relaxivity values employ obtaining S/V value from Eq. 7 by nitrogen adsorption, cation exchange capacity, or image analysis (Hürlimann et al. 2002; Coates et al. 1999; Fleury 2007). Another way is to match the received distributions with results of MIP and μ CT, which makes the NMR results highly built upon the other methods. Values of surface relaxivity coefficient for different rocks are reported in many recent studies; the average value obtained experimentally varies from 2 to 14 $\mu\text{m/s}$. In the current study, we present results on PSD by two selected values for carbonate rocks (5 $\mu\text{m/s}$ and 10 $\mu\text{m/s}$) and attempt to analyze the influence of this coefficient on the comparison of various methods.

3 Results and Discussion

3.1 Gas Porosimetry and Permeametry Results

The porosity and permeability of the rock sample toward nitrogen gas were determined as 23.0% and 20 mD, respectively.

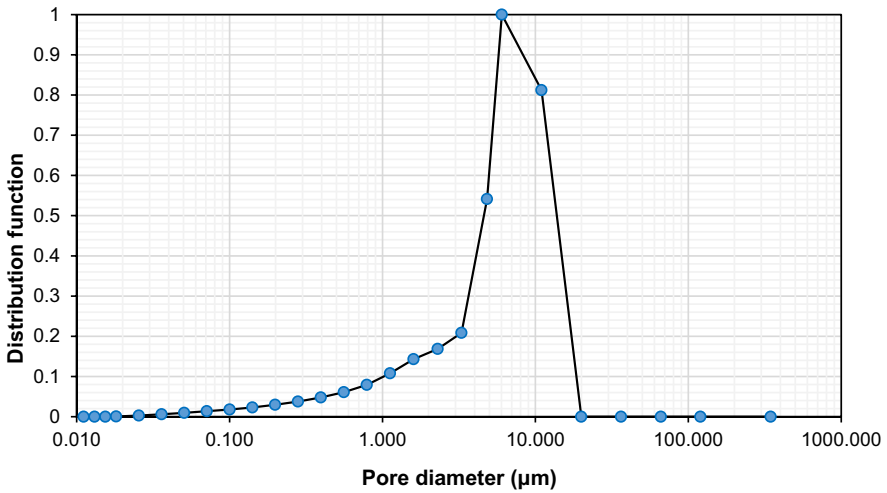


Fig. 4 Pore size distribution obtained by MIP in terms of normalized $\left(\frac{dv}{d\log(r)}\right)$ versus pore diameter

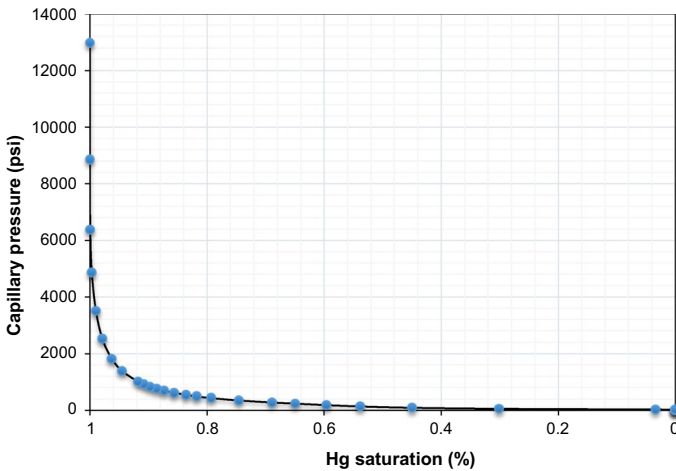


Fig. 5 Capillary pressure versus Hg saturation obtained by MIP

3.2 Results of MIP

The pore access diameter obtained from this technique is presented in Fig. 4. The mean diameter of the pores is about 5 μm. This method is unable to distinguish pores and throats. The porosity obtained from the MIP technique is around 17.23%. The difference between the estimation of MIP (17.23%) and the one obtained by gas porosimetry (23%) could be due to the pores, which are accessible to gas but not mercury. The permeability by MIP is around 18.42 mD, which is close to that obtained by gas permeameter (20 mD). The capillary pressure curve versus Hg saturation is presented in Fig. 5. This is the advantage of the MIP method compared to other aforementioned methods. Based on the capillary

pressure–saturation curve, the volume fraction–size distribution is obtained and illustrated in Fig. 6.

3.3 Results of μ CT

Imaging by means of computed tomography can be performed under different resolutions or voxel size. Starting with an original core (e.g., 40 mm diameter), we can analyze the entire sample but under limited resolution (not better than 20 $\mu\text{m}/\text{voxel}$). However, this would be enough to estimate the general quality of the sample: homogeneity, presence, number, and orientation of fractures, as well as the porous structure and minerals distribution based on X-ray attenuation coefficients. Big pores larger than 40–50 μm would be visible, but others will be either unresolved or partially resolved. For the case of tight formations or carbonates, this resolution is insufficient to analyze porous structure adequately: for tight formations, most of the pore sizes are below this number, while for carbonates, even with some large pores easily identified, we might not just lose porosity related to small pores and channels but also lose connectivity of the porous structure. In order to increase resolution, the scanning of the central part of the sample and smaller region of interest (ROI) could be performed, or smaller samples could be drilled out of the original sample for higher resolution scanning. The way with ROI scanning can increase resolution usually up to 3 times and would not require damaging operations (e.g., coring smaller samples) within a sample. The drawbacks of this approach are related to the big “filter” formed of the material out of ROI. It attenuates most of the energy and decreases the signal-to-noise ratio. Additionally, the tube power should be reduced to match the size of the focal spot with higher resolution, while the magnification mainly would be increased by moving the detector to the back due to restrictions of placing the sample closer to the X-ray tube. As a result, the scanning time increases significantly with a noisy image. It is also hard to position ROI, and usually, this type is done along the rotation axis of the sample. Coring a smaller sample from the specified place is a preferable way to increase the resolution of the 3D image and sample structure. Taking a higher resolution image from a small part of the original sample may provide more precise information about the recorded structure. Still, this information may not be representative of the original sample due to its

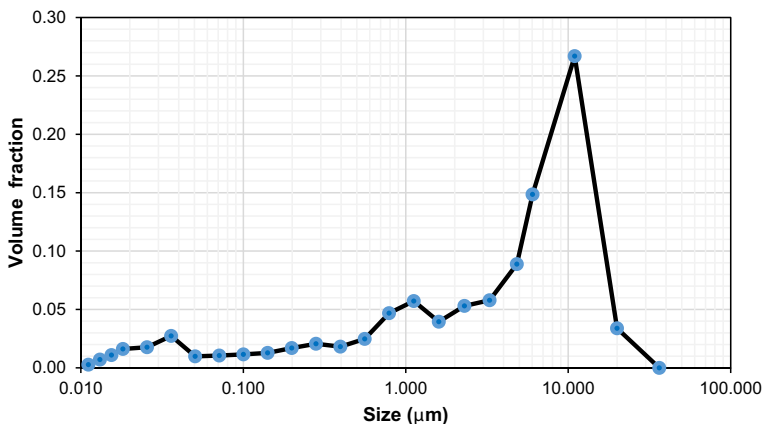


Fig. 6 Volume fraction versus pore diameter by MIP

possible inhomogeneity. In that case, a correlation between size and properties should be analyzed. Same applies to the size of the array for processing with software. The analysis of large-size image files is computationally demanding. On the other hand, smaller file size risks losing the information content (i.e., porous skeleton information). Therefore, comparing microtomography at different resolutions and sizes of the array can shed light on the amount of information lost and differences in porous media characterization associated with the size of the array and voxel size.

In this section, the comparison of results from μ CT scanning at voxel sizes of $27.5\ \mu\text{m}$ and $5\ \mu\text{m}$ has been provided. Figure 7 shows the porous structure of the rock sample obtained by this technique at $27.5\ \mu\text{m}/\text{voxel}$ and in Fig. 8 for $5\ \mu\text{m}/\text{voxel}$ portraying pores divided into open and closed ones. Table 1 presents the analysis of μ CT images in terms of total, closed, and open porosity obtained from scans with 27.5 and $5\ \mu\text{m}/\text{voxel}$. The segmentation for pores and mineral skeleton was performed by an automatic OTSU algorithm. The array size for both scans is quite close in terms of the number of voxels but significantly differs in geometrical size: the volume analyzed at resolution $27.5\ \mu\text{m}/\text{voxel}$ is about 120 times bigger than for $5\ \mu\text{m}/\text{voxel}$ one. The minimal directly detectable pore size for a coarse scan is about $40\text{--}50\ \mu\text{m}$. Still, a significant part of porosity is under that number illustrated by detectable overall porosity for two resolutions and ratio of overall to open porosity. The overall porosity for fine resolution scan at $5\ \mu\text{m}/\text{voxel}$ is 21.5%, and pretty close to one measured by gas pycnometer (23%), revealing most of the porosity lies within the range above $7\ \mu\text{m}$, detectable at $5\ \mu\text{m}/\text{voxel}$ resolution. The resolution of μ CT, however, limits to pores bigger than 1 micron, and thereby, prevents it from obtaining a precise

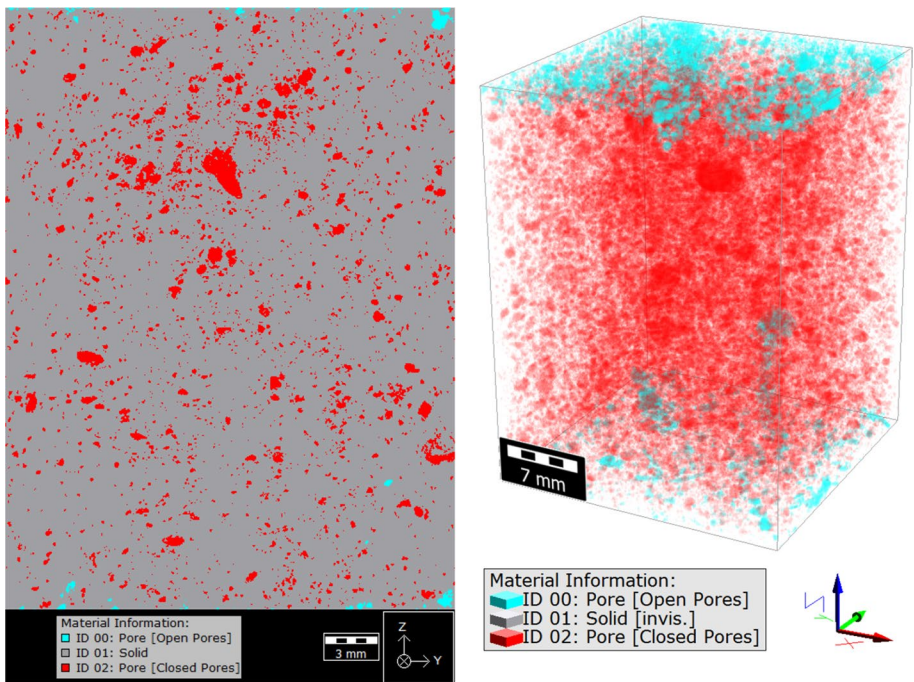


Fig. 7 The porous structure of a rock sample by μ CT imaging ($27.5\ \mu\text{m}$ resolution). Slice (left) and 3D segmented image with open and closed porosity

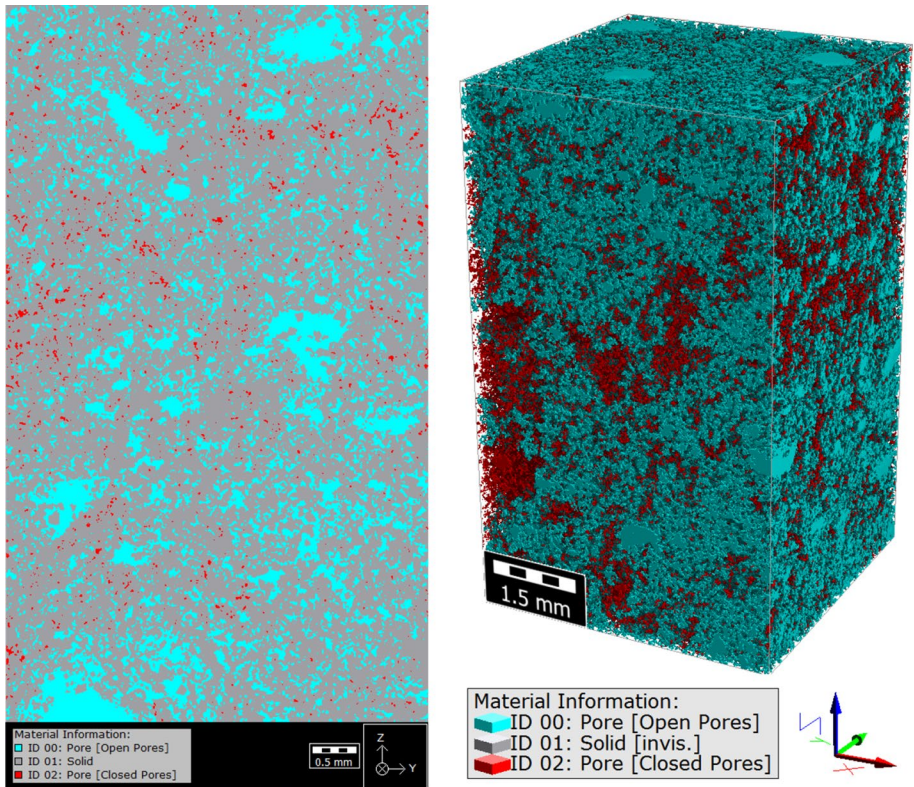


Fig. 8 The porous structure of a rock sample by μ CT imaging ($5\ \mu\text{m}$ resolution). Slice (left) and 3D segmented image with open and closed porosity

Table 1 μ CT (27.5 and $5\ \mu\text{m}$ /voxel resolution) pore structural analysis results

Scan resolution	$27.5\ \mu\text{m}/\text{voxel}$	$5\ \mu\text{m}/\text{voxel}$
Processed array (voxel)	$965 \times 965 \times 1290$	$1000 \times 1000 \times 1700$
Processed array (mm)	$26.54 \times 26.54 \times 35.48$	$5 \times 5 \times 8.5$
Overall porosity (%)	8.19	21.49
Open porosity (%)	0.65	20.37
Closed porosity (%)	7.55	1.12

porosity value, although it is able to distinguish close porosity and open porosity, which is not a feasible task for the other methods. The closed porosity is 1.1% for a $5\ \mu\text{m}/\text{voxel}$ scan, but this may also be connected porosity at a level below the resolution of the scan.

In contrast to $5\ \mu\text{m}/\text{voxel}$ data, scan at $27.5\ \mu\text{m}/\text{voxel}$ shows that overall porosity is just 8.2%, and most of it (7.6%) is closed. The open and closed porosity visualization in Figs. 7 and 8 shows the distribution of open and closed porosity identified for both resolutions by analysis of pores connectivity from Z+ and Z- planes. The structure of a fine resolution scan is permeable from one plane to another, while very limited connectivity can be

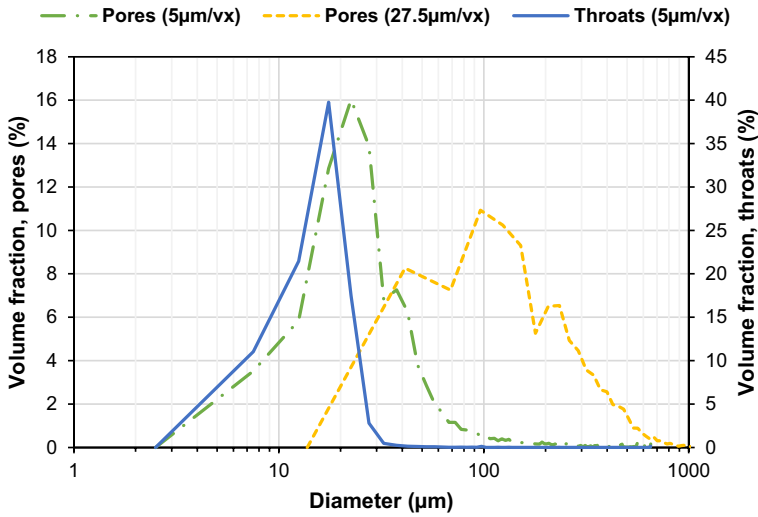


Fig. 9 Pore size distribution obtained by the geometric method calculated from images with 5 µm/voxel and 27.5 µm/voxel as well as pore throats for images with 5 µm/voxel

identified by the coarse scan. The pore size distribution for both resolutions is presented in Fig. 9, together with pore throats size distribution from 5 µm/voxel data. The analysis for pore throats size distribution is meaningless for lower resolution since most of the pores are identified as disconnected due to the lost connectivity information.

The characteristic diameters for pores occupying overall 10, 50, and 90% of porosity space are presented in Table 2. The absence of small pores for coarse scan analysis refers to the undetectability of these species. In fact, the inhomogeneity of the sample requires significantly larger volumetric array for analysis and, therefore, results in low resolution. The throats size distribution for 5 µm/voxel shows a very narrow peak in the range of 10–30 µm, and that is why identified porous structure at 27.5 µm/voxel scan is almost not connected.

Different approaches can, however, be employed to analyze µCT images, some of which are implemented in the available porous media image analysis tools. Each method would provide the user with a different result based on the interpretations and assumptions behind the technique. For instance, GeoDict performs two analyses. The geometric method used in GeoDict results in the pore size distribution. The other method uses the pore morphology technique [see (Hilpert and Miller 2001) and (Sweijen et al. 2017) for details] to simulate non-wetting phase invasion and to model the mercury porosimetry experiment (virtually) to obtain throat size distribution.

Table 2 The characteristic diameter of the pores by µCT imaging (27.5 µm and 5 µm resolution)

Scan resolution	27.5 µm/voxel	5 µm/voxel
Characteristic diameter	Pores	
D10	61.6 µm	15.2 µm
D50	186 µm	29.2 µm
D90	473 µm	117 µm

Furthermore, μ CT offers the possibility to estimate the surface properties of the porous medium. The specific surface area of the rock porous skeleton has been estimated as $28.41 \text{ m}^2/\text{m}^3$ based on the μ CT images.

3.4 Results of NMR

The incremental volume of pores versus the pore radius obtained from this method on the kerosene saturated sample is presented in Fig. 10. Fluid volume by NMR is used to calculate sample porosity, and the plug volume is estimated by geometrical size. The pore size distribution is generated based on the T_2 relaxation curve. Fluid volume and NMR porosity are presented in Table 3.

NMR permeability is calculated using the cutoff Coates model based on the T_2 data (effective porosity value) and FFI and BVI indexes, which are determined after NMR analysis of the centrifuged sample and setting the T_2 cutoff value. T_2 cutoff is typically set by spectral analysis of the T_2 curves for both 100% saturated sample and in a state of irreducible saturation. The high amount of large voids and insignificant volume of bound fluids affects and complicates the T_2 cutoff estimation resulting in the range of 16–90 ms (depends on calculation method). Thus, the NMR method leads to a large overestimation of the sample permeability and, therefore, does not provide a reliable measurement. Regarding permeability, while the NMR technique results in an out of range permeabilities, highly

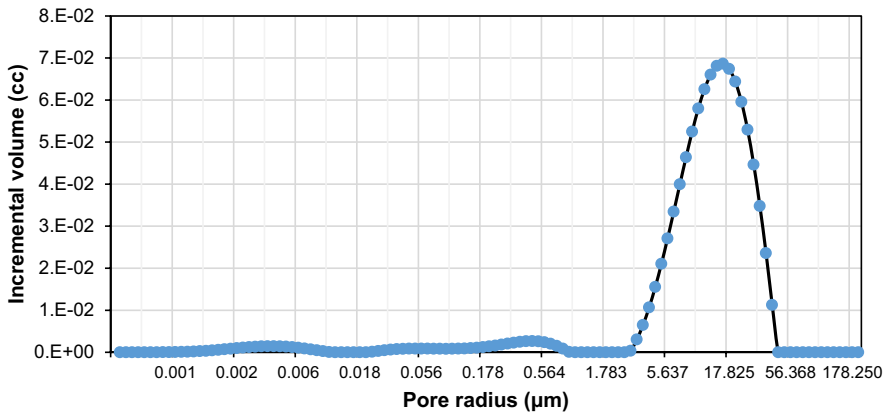


Fig. 10 Pore size distribution obtained by NMR for a sample at a 100% kerosene saturation state ($\rho = 10 \text{ } \mu\text{m/s}$)

Table 3 Fluid volume by NMR

As-received		Dried		Saturated		Fluid
NMR fluid volume	Porosity by NMR	NMR fluid volume	Porosity by NMR	NMR fluid volume	Porosity by NMR	
cc	%	cc	%	cc	%	
0.38	0.83	0.34	0.75	9.89	21.40	kerosene

dependent on the cutoff range used, namely 422 mD, the permeability obtained by MIP is around 18.42 mD, close to that obtained by gas permeameter (20 mD).

3.5 Comparing Various Methods of Porous Media Characterization

A comparison of the obtained values for the porosity from different methods is presented in Fig. 11.

The porosity by gas porosimetry is considerably different from that obtained by μ CT scan at low resolution with 27.5 $\mu\text{m}/\text{voxel}$ size. Under that insufficient resolution, an important part of porosity with characteristic size below 40–50 μm is missing, resulting in low recoverable porosity and losing pores connectivity. Choosing scan resolution adequate to the scale of porous structure and taking an image of a representative volume of the sample are the key elements for correct CT scan and analysis. Besides these limitations, the μ CT, however, provides the opportunity to measure pore and throat size distribution directly, to obtain open and closed porosity, the coordination number of pores and surface and volume characteristics of the porous medium, which can hardly be performed through other techniques.

The porosity obtained from μ CT (21.5%) is closer than the overall porosity obtained by MIP (17.23%) to the gas porosimetry result (23%). The 5% difference could be due to inaccessible pores to mercury, which can be accessible to nitrogen with much smaller molecules.

The porosity obtained from NMR is 21.4%. This value shows a good correlation with the results of μ CT scanning. However, it is lower than porosity values by μ CT (5 $\mu\text{m}/\text{voxel}$) and by gas injection. It can be explained by the presence of large voids (caverns) which are not occupied by the saturating fluid and thereafter not detected by NMR. In relation to MIP results, NMR provides a higher value of total rock porosity, which confirms the underestimation of bulk porosity by mercury intrusion porosimetry. Overall, the NMR technique demonstrates a reliable measurement of rock saturation and porosity. However, the application of NMR is conditioned by the probe preparation (rock cleaning and saturation procedure) as well as the rock void space specifics (e.g., the presence of open caverns).

The normalized volume fraction of pores and throats and the cumulative volume fractions are presented in Figs. 12 and 13, respectively.

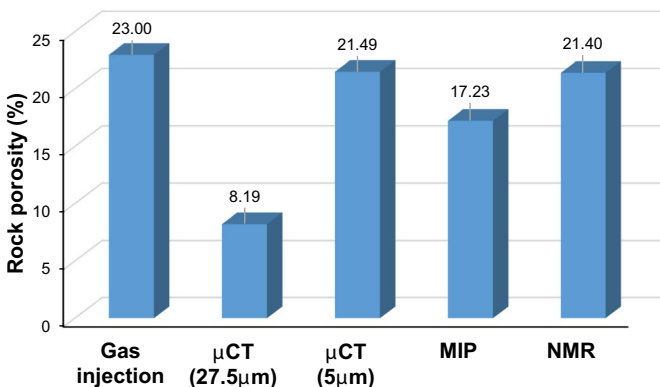


Fig. 11 The porosity of the rock sample obtained by various methods

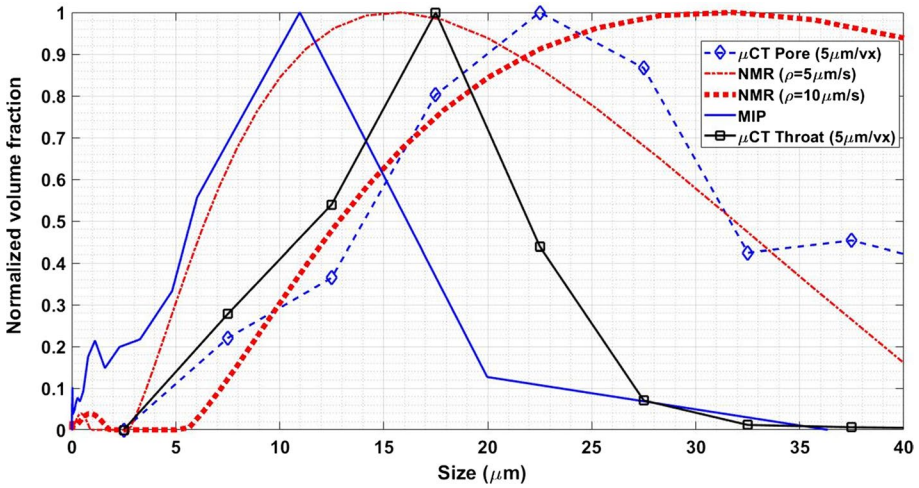


Fig. 12 Normalized volume fraction obtained from various techniques

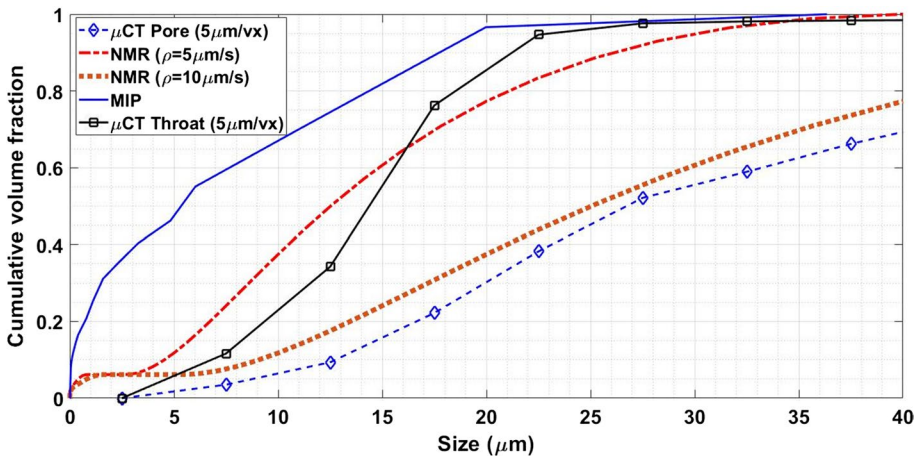


Fig. 13 Cumulative volume fractions by various methods

In the framework of comparison of different methods, we introduce the results of basic statistical comparison of PSD obtained by various methods. The cumulative probability function distribution (CDF) of the so-called generalized inverse Weibull distribution (GIW) has been found to be of the closest match to the experimental cumulative volume fractions and therefore has been used for comparison. GIW distribution parameters are reported in Table 4. The CDF of GIW is formulated as follows (De Gusmao et al. 2011):

$$G(x) = \exp \left[-c \left(\frac{a}{x} \right)^b \right], \tag{8}$$

where a , b , and c are GIW parameters and take positive values.

Table 4 Parameters of the generalized inverse Weibull distribution

Parameter/method	GIW distribution parameter			Error measure of fit R^2
	<i>a</i>	<i>b</i>	<i>c</i>	
μ CT pore size distribution	13.61	1.38	1.81	0.99
NMR ($\rho = 5 \mu\text{m/s}$)	9.70	1.80	0.92	0.99
NMR ($\rho = 10 \mu\text{m/s}$)	13.88	1.80	1.69	0.99
MIP	1.36	1.34	1.35	0.79
μ CT throat size distribution	10.26	4.36	2.55	0.99

Table 5 presents the minimum, maximum, and median values of pore and throat radii detected by various techniques.

Based on the estimated CDFs of the results, in order to use the Kolmogorov–Smirnov method to compare the CDFs, the estimated CDFs are partitioned into 50 points, and the maximum distance between them is measured and reported hereafter (Fig. 14).

As can be seen in Fig. 14, the coefficient of surface relaxivity in the NMR analysis plays a great role in the final result. The coefficients used in our study are in the range

Table 5 The minimum, maximum, and median pore and throat radii as determined from various techniques

Method	Min (nm)	Max (μm)	Median* (μm)
μ CT pore size distribution	7500	652.50	27.33
NMR ($\rho = 5 \mu\text{m/s}$)	0.20	200	11.38
NMR ($\rho = 10 \mu\text{m/s}$)	0.40	400	22.76
MIP	20	19.97	3.32
μ CT throat size distribution	7500	652.50	13.84

*The median value has been calculated based on the cumulative volume fraction–size distributions whose parameters are presented in Table 4

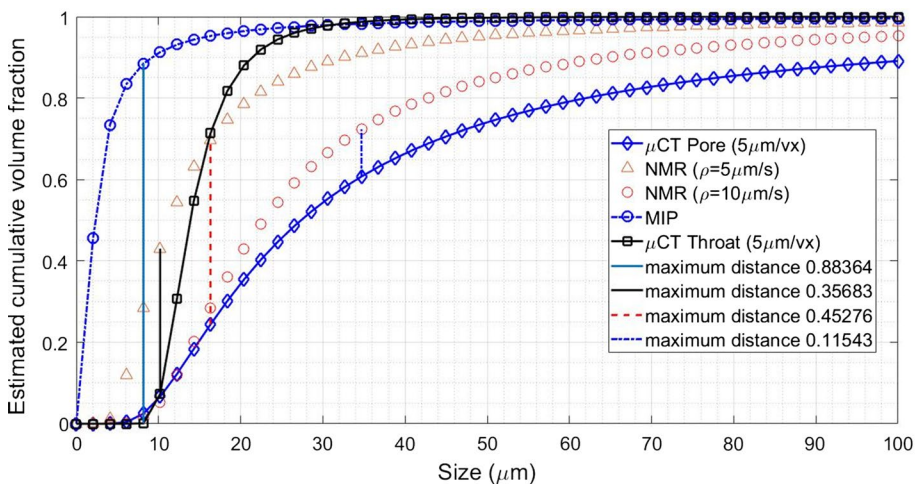


Fig. 14 Distance between the cumulative volume fractions (cumulative distributions)

reported in the literature for carbonate rocks. The coefficient of $10 \mu\text{m/s}$ yields in the best estimation of pore size distribution with the maximum distance of 0.11543 for 50 points, which is reasonably below that the critical value of the Kolmogorov–Smirnov method for 50 points ($1.36/\sqrt{50}=0.1923$, for 95% confidence interval). A lower choice for this coefficient, namely $5 \mu\text{m/s}$, results in an estimation of the CDF of throat volume fraction–size distribution rather than pore volume fraction. This shows the importance of the selection of the surface relaxivity coefficient for the correct calculation of PSD by the NMR method. The reason behind this behavior in NMR analysis is that the results of NMR contain the effect of resonance of hydrogen atoms in all parts of the porous volume, and not only pores. Therefore, the resulting NMR volume fraction distributions appear in close vicinity of pore size distribution and throat size distributions.

Furthermore, when examined in light of Kolmogorov–Smirnov distances, MIP, which uses the bundle of tube assumption, gives neither a good approximation of pore volume fraction–size distribution nor that of throats. The reason is assigning both functions of pores and throats to an idealized cylindrical capillary tube in MIP. This method assumes all pores of a certain size are drained at once when the capillary pressure associated with that tube radius has overcome, while in reality, all pores of the same size (as well as the throats of the same size) may remain saturated until higher capillary pressure level, when some pores or throats of smaller size which are in their path to the drainage front have been drained. That is to say, the loss of connectivity in the common bundle of capillary conceptualization used in MIP leads to an estimation of the so-called pore access size distribution, which is neither representative of that of pores nor the throats. Although it is closer to the throat volume–fraction distribution, by no means its resulting distribution is an acceptable one; it assigns much of the volumes to the considerably smaller sizes.

In current work, we have attempted to analyze the applicability and limitations of a suite of both state-of-the-art techniques, including NMR, MIP, μCT , and conventional methods such as gas injection based on pressure decay (PDP). All the mentioned techniques have their own advantages and limitation, which we shortly stated in Table 6.

In the current study, due to the limited core material, we analyzed the most representative experimental methods for the porous structure investigation. For open (bulk) porosity determination, any of NMR, μCT , or conventional gas injection (PDP) is recommended. Therefore, for precise investigation of the rock effective porosity, it is important to control the CT resolution and maintain it at its highest level. For obtaining PSD (pore radius or diameter), both NMR and X-ray CT provide reliable results; the raw data processing is essential and should be carefully tuned. Based on our results, pore throat size is well characterized by μCT ($5 \mu\text{m}/\text{voxel}$), while the MIP leads to an underestimation of the values. Thus, the scope of application of each method according to our results can be described as follows (see also Table 6):

- Gas injection-based method demonstrates reliable and efficient measurement of open/bulk porosity and permeability; it is recommended for preliminary estimation of rock reservoir properties.
- For a detailed picture of the rock porous structure, the combination of several methods (NMR, MIP, and CT) is required. In the absence of X-ray CT, one could use NMR for obtaining pore size distribution and MIP for throat size distribution. It should, however, be noted that both methods underestimate the targeted distributions, as revealed in this study.

Table 6 Summary of methods

Method	Parameter	Advantages	Limitations
Gas injection/PDP	Open porosity	Availability of the method (ease of use) Noninvasiveness	Not suitable for rock with permeability less than 0.5 mD
NMR	Open and closed porosity PSD	Integral core characterization (open and closed porosity) Advanced spatial profiling Noninvasiveness	Dependence on the surface relaxivity coefficient Limited resolution in the submicron range
X-ray CT	Open and closed porosity PSD/throat size	Direct pore space visualization, the considerable potential for digital rock analysis, sample quality (homogeneity, fractures) control	Resolution-driven analysis
MIP	Open and connected porosity A rough estimation of pore throat size	Wide range of detected pore sizes	Hazardousness of the experimental procedure Underestimation of the porous system parameters

- The permeability by gas is more accurate and reliable than that by NMR calculation; additional research involving more experimental techniques for measuring permeability may form a basis for a separate publication.
- The resulting pore size distribution from MIP is rather a rough estimation of the throat size distribution obtained from μ CT (5 $\mu\text{m}/\text{voxel}$), while NMR prediction can provide a rather good approximation of the pore size distribution obtained from μ CT (5 $\mu\text{m}/\text{voxel}$). One should note that NMR prediction is highly sensitive to the surface relaxivity coefficient considered in the analysis.
- For complex porous systems (such as carbonate rocks) even at a given high porosity and permeability, it is difficult to choose one approach yielding the best estimation of all porous media characteristics, namely porosity, permeability and pore, as well as throat size distribution. Therefore, the joint application of them is recommended (i.e., NMR + μ CT for pore size, MIP + NMR + Gas (porosimeter) for porosity and Gas (permeameter) + MIP for permeability, and finally μ CT for throat size distribution, and in its absence, alternatively MIP).

Although care was taken to distinguish between pores and throats in our porous media characterization, making it superior to the previously published studies in this regard, and furthermore a suite of different techniques was utilized, one should note that due to the complex nature of porous media in different rocks, it is suggested to perform further studies on other rock types such as shales and sandstones in order to gain full insight on the scope of application of these techniques in different rock types. Specific properties of each type of rock (high porosity for sandstone and low porosity, the presence of viscous components, and kerogen in shales) may result in significant changes in comparison and analysis of utilized techniques. At given conditions, we have attempted to focus on the most recognized experimental techniques and perform all the measurements on the single (target) rock sample divided into multiple specimens and utilized according to the proposed workflow. The limited core material is one of the crucial issues in the area of experimental petrophysics which highlights the value of a simultaneous detailed and integrated study on a single core sample. Further steps of our research involve enhancing the number of utilized experimental techniques such as SEM, FIB–SEM, FIB–HIM, and low-temperature nitrogen adsorption for investigation of the nano- and micropores in the rock.

4 Summary and Conclusions

In this study, a thorough analysis of the porous skeleton of rock samples was conducted by means of various state-of-the-art techniques. The following conclusions can be made:

- While μ CT data if analyzed, directly, can reveal a realistic portrayal of the porous skeleton; the pore size distribution obtained from MIP is considerably different from real pore size distribution. It can give a different description of the porous structure, which would, potentially, result in the erroneous predictions of flow and transport properties, if it is used for post-processing. On the other hand, NMR can result in a rather good prediction of pore size distribution. The surface relaxivity coefficient, however, strongly influences the analysis result.
- MIP would rather provide a rough estimation of the throat size distribution, which without pore size distribution fails to give a complete characterization of the porous

skeleton. Therefore, either the bundle of capillary conceptualization used to interpret MIP technique has to be modified to result in both pore and throat size distributions or imaging has to be considered as an inevitable part of any porous media characterization process. However, one should note that the imaging has to be performed at a suitable resolution not to miss the porosity inherent in smaller scales and smaller-scale heterogeneities.

- The NMR technique, gas injection, and μ CT imaging can all be utilized, provided that only bulk measures of the porous skeleton, such as porosity, are required to be determined. Mercury intrusion porosimetry gives an underestimation of porosity as compared to the other methods, and coarse μ CT scan imaging due to almost sixfold higher resolution loses a considerable amount of information on hidden porosity. Its estimated porosity is almost one-third of the porosity estimated by the other techniques.
- Regarding permeability estimation, NMR is, however, less reliable as its results are highly dependent on the cutoff level and completely different from methods such as gas injection and MIP. The definition of permeability by Coates equation employs the values of free and bound fluid volumes and leads to an overestimation of permeability due to initially high free fluid index and not reliable experimental T_2 cutoff determination. The latter two (gas injection and MIP) are resulting in almost similar permeability.

Acknowledgements The enhanced oil recovery laboratories of Shiraz University, Skoltech University, and Abdal Industrial Project Management Co. (MAPSA) are gratefully acknowledged for the collaboration in performing rock sampling, CT, NMR, MIP, XRD, and gas injection experiments. Furthermore, authors acknowledge the constructive comments of anonymous reviewers, which improved the manuscript significantly.

References

- Abragam, A., Abragam, A.: *The Principles of Nuclear Magnetism*. Oxford University Press, Oxford (1961)
- Adebayo, A.R., Kandil, M.E., Okasha, T.M., Sanni, M.L.: Measurements of electrical resistivity, NMR pore size and distribution, and X-ray CT-scan for performance evaluation of CO₂ injection in carbonate rocks: a pilot study. *Int. J. Greenh. Gas Control* **63**, 1–11 (2017)
- Adler, P.M., Jacquin, C.G., Quiblier, J.A.: Flow in simulated porous media. *Int. J. Multiph. Flow* **16**(4), 691–712 (1990)
- Alqahtani, N., Alzubaidi, F., Armstrong, R.T., Swietojanski, P., Mostaghimi, P.: Machine learning for predicting properties of porous media from 2d X-ray images. *J. Petrol. Sci. Eng.* **184**, 106514 (2020)
- Armstrong, R.T., McClure, J.E., Robins, V., Liu, Z., Arns, C.H., Schlüter, S., Berg, S.: Porous media characterization using minkowski functionals: theories, applications and future directions. *Transp. Porous Media* **130**(1), 305–335 (2019)
- Arns, C.H., Knackstedt, M.A., Martys, N.S.: Cross-property correlations and permeability estimation in sandstone. *Phys. Rev. E* **72**, 46304 (2005)
- Benavides, F., Leiderman, R., Souza, A., Carneiro, G., de Vasconcellos Azeredo, R.B.: Pore size distribution from NMR and image based methods: a comparative study. *J. Pet. Sci. Eng.* **184**, 106321 (2020)
- Bloembergen, N., Purcell, E.M., Pound, R.V.: Relaxation effects in nuclear magnetic resonance absorption. *Phys. Rev.* **73**, 679 (1948)
- Bryant, S., Cade, C., Mellor, D.: Permeability prediction from geologic models. *Am. Assoc. Pet. Geol. Bull.* **77**, 1338–1350 (1993)
- Büttner, J.: Permeability of young sea ice from microtomographic images. M.Sc. thesis, Geophysical Institute, University of Bergen, Bergen, Norway (2011)
- Callaghan, P.T.: *Principles of Nuclear Magnetic Resonance Microscopy*. Oxford University Press on Demand, Oxford (1993)
- Cnudde, V., Boone, M.N.: High-resolution X-ray computed tomography in geosciences: a review of the current technology and applications. *Earth Sci. Rev.* **123**, 1–17 (2013)


- Coates, G.R., Xiao, L., Prammer, M.G.: NMR Logging Principles and Applications. Halliburton Energy Services Publication, Houston (1999)
- De Gusmao, F.R., Ortega, E.M., Cordeiro, G.M.: The generalized inverse Weibull distribution. *Stat. Pap.* **52**(3), 591–619 (2011)
- Dejam, M., Hassanzadeh, H.: The role of natural fractures of finite double-porosity aquifers on diffusive leakage of brine during geological storage of CO₂. *Int. J. Greenh. Gas Control* **78**, 177–197 (2018a)
- Dejam, M., Hassanzadeh, H.: Diffusive leakage of brine from aquifers during CO₂ geological storage. *Adv. Water Resour.* **111**, 36–57 (2018b)
- Feia, S., Ghabezloo, S., Bruchon, J.-F., Sulem, J., Canou, J., Dupla, J.-C.: Experimental evaluation of the pore-access size distribution of sands. *Geotech. Test. J.* **37**, 613–620 (2014)
- Fleury, M.: NMR surface relaxivity determination using NMR apparent diffusion curves and BET measurements. In: International Symposium of the Society of Core Analysts (pp. 10–12). Canada: Calgary. Available online at: <http://jgmaas.com/SCA/2007/35.pdf> (2007)
- Franc, J., Guibert, R., Horgue, P., Debenest, G., Plouraboué, F.: Image-based effective medium approximation for fast permeability evaluation of porous media core samples. *Comput. Geosci.* **24**, 1–13 (2020)
- Fredrich, J.T.: 3D imaging of porous media using laser scanning confocal microscopy with application to microscale transport processes. *Phys. Chem. Earth Part A.* **24**(7), 551–561 (1999)
- Gao, F., Song, Y., Li, Z., Xiong, F., Chen, L., Zhang, X., Chen, Z., Moortgat, J.: Quantitative characterization of pore connectivity using NMR and MIP: a case study of the Wangyinpu and Guanyintang shales in the Xiuyu basin, Southern China. *Int. J. Coal Geol.* **197**, 53–65 (2018)
- Gao, H., Wang, C., Cao, J., He, M., Dou, L.: Quantitative study on the stress sensitivity of pores in tight sandstone reservoirs of Ordos basin using NMR technique. *J. Pet. Sci. Eng.* **172**, 401–410 (2019)
- Gharedaghloo, B., Price, J.S., Rezaeezhad, F., Quinton, W.L.: Evaluating the hydraulic and transport properties of peat soil using pore network modeling and X-ray micro computed tomography. *J. Hydrol.* **561**, 494–508 (2018)
- Ghomeshi, S., Kryuchkov, S., Kantzas, A.: An investigation into the effects of pore connectivity on T_2 NMR relaxation. *J. Magn. Reson.* **289**, 79–91 (2018)
- Hernández Zubeldia, E., de SM Ozelim, L.C., Luís Brasil Cavalcante, A., Crestana, S.: Cellular automata and X-ray microcomputed tomography images for generating artificial porous media. *Int. J. Geomech.* **16**(2), 04015057 (2016)
- Hidajat, I., Rastogi, A., Singh, M., Mohanty, K.K.: Transport properties of porous media reconstructed from thin-sections. *SPE J.* **7**(01), 40–48 (2002)
- Hilpert, M., Miller, C.T.: Pore-morphology-based simulation of drainage in totally wetting porous media. *Adv. Water Resour.* **24**, 243–255 (2001)
- Hou, D., Li, D., Hua, P., Jiang, J., Zhang, G.: Statistical modelling of compressive strength controlled by porosity and pore size distribution for cementitious materials. *Cem. Concr. Compos.* **96**, 11–20 (2019)
- Hürlimann, M.D., Venkataraman, L., Flaum, C., Speier, P., Karmonik, C., Freedman, R., Heaton, N.: Diffusion-Editing: New NMR Measurement of Saturation and Pore Geometry, SPWLA 43rd Annual Logging Symposium (2002)
- Kamrava, S., Tahmasebi, P., Sahimi, M.: Linking morphology of porous media to their macroscopic permeability by deep learning. *Transp. Porous Media* **131**(2), 427–448 (2020)
- Kim, F.H., Penumadu, D., Schulz, V.P., Wiegmann, A.: Pore size distribution and soil water suction curve from micro-tomography measurements and real 3-D digital microstructure of a compacted granular media by using direct numerical simulation technique. In: Laloui, L., Ferrari, A. (eds.) *Multiphysical Testing of Soils and Shales*, pp. 171–176. Springer (2013)
- Klaver, J., Desbois, G., Littke, R., Urai, J.L.: BIB-SEM characterization of pore space morphology and distribution in postmature to overmature samples from the Haynesville and Bossier Shales. *Mar. Pet. Geol.* **59**, 451–466 (2015)
- Li, Y., Zhang, C., Tang, D., Gan, Q., Niu, X., Wang, K., Shen, R.: Coal pore size distributions controlled by the coalification process: an experimental study of coals from the Junggar, Ordos and Qinshui basins in China. *Fuel* **206**, 352–363 (2017)
- Li, X., Kang, Y., Haghighi, M.: Investigation of pore size distributions of coals with different structures by nuclear magnetic resonance (NMR) and mercury intrusion porosimetry (MIP). *Measurement* **116**, 122–128 (2018)
- Ma, X., Guo, S., Shi, D., Zhou, Z., Liu, G.: Investigation of pore structure and fractal characteristics of marine-continental transitional shales from Longtan Formation using MICP, gas adsorption, and NMR (Guizhou, China). *Mar. Pet. Geol.* **107**, 555–571 (2019)

- Moro, F., Böhni, H.: Ink-bottle effect in mercury intrusion porosimetry of cement-based materials. *J. Colloid Interface Sci.* **246**, 135–149 (2002)
- Morriss, C., Rossini, D., Straley, C., Tutunjian, P., Vinegar, H.: Core Analysis By Low-field NMR. The Log Analyst (Society of Petrophysicists and Well-Log Analysts), 38(2), Document ID: SPWLA-1997-v38n2a3. Available online at: <https://www.onepetro.org/journal-paper/SPWLA-1997-v38n2a3>.
- Mostaghimi, P., Blunt, M.J., Bijeljic, B.: Computations of absolute permeability on micro-CT images. *Math. Geosci.* **45**(1), 103–125 (2013)
- Mourzenko, V.V., Thovert, J.F., Adler, P.M.: Trace analysis for fracture networks with anisotropic orientations and heterogeneous distributions. *Phys. Rev. E* **83**(3), 031104 (2011)
- Øren, P.E., Bakke, S.: Process based reconstruction of sandstones and prediction of transport properties. *Transp. Porous Media* **46**(2–3), 311–343 (2002)
- Qiu, X., Tan, S.P., Dejam, M., Adidharma, H.: Experimental study on the criticality of a methane/ethane mixture confined in nanoporous media. *Langmuir* **35**, 11635–11642 (2019a)
- Qiu, X., Tan, S.P., Dejam, M., Adidharma, H.: Simple and accurate isochoric differential scanning calorimetry measurements: phase transitions for pure fluids and mixtures in nanopores. *Phys. Chem. Chem. Phys.* **21**, 224–231 (2019b)
- Qiu, X., Tan, S.P., Dejam, M., Adidharma, H.: Isochoric measurement of the evaporation point of pure fluids in bulk and nanoporous media using differential scanning calorimetry. *Phys. Chem. Chem. Phys.* **22**, 7048–7057 (2020)
- Remeysen, K., Swennen, R.: Application of microfocus computed tomography in carbonate reservoir characterization: possibilities and limitations. *Mar. Pet. Geol.* **25**, 486–499 (2008)
- Rezaei, A., Abdollahi, H., Derikvand, Z., Hemmati-Sarapardeh, A., Mosavi, A., Nabipour, N.: Insights into the effects of pore size distribution on the flowing behavior of carbonate rocks: linking a nano-based enhanced oil recovery method to rock typing. *Nanomaterials* **10**, 972 (2020)
- Song, S.-B., Liu, J.-F., Yang, D.-S., Ni, H.-Y., Huang, B.-X., Zhang, K., Mao, X.-B.: Pore structure characterization and permeability prediction of coal samples based on SEM images. *J. Nat. Gas Sci. Eng.* **67**, 160–171 (2019)
- Spanne, P., Thovert, J.F., Jacquin, C.J., Lindquist, W.B., Jones, K.W., Adler, P.M.: Synchrotron computed microtomography of porous media: topology and transports. *Phys. Rev. Lett.* **73**(14), 2001 (1994)
- Sweijen, T., Aslannejad, H., Hassanizadeh, S.M.: Capillary pressure–saturation relationships for porous granular materials: pore morphology method vs. pore unit assembly method. *Adv. Water Resour.* **107**, 22–31 (2017)
- Tan, S.P., Qiu, X., Dejam, M., Adidharma, H.: Critical point of fluid confined in nanopores: experimental detection and measurement. *J. Phys. Chem. C* **123**, 9824–9830 (2019)
- Thovert, J.F., Salles, J., Adler, P.M.: Computerized characterization of the geometry of real porous media: their discretization, analysis and interpretation. *J. Microsc.* **170**(1), 65–79 (1993)
- Thovert, J.F., Yousefian, F., Spanne, P., Jacquin, C.G., Adler, P.M.: Grain reconstruction of porous media: application to a low-porosity Fontainebleau sandstone. *Phys. Rev. E* **63**(6), 061307 (2001)
- Timur, A.: Effective porosity and permeability of sandstones investigated through nuclear magnetic resonance principles. In: SPWLA 9th Annual Logging Symposium. Society of Petrophysicists and Well-Log Analysts (1968)
- Tinet, A.J., Corlay, Q., Collon, P., Golfier, F., Kalo, K.: Comparison of various 3D pore space reconstruction methods and implications on transport properties of nanoporous rocks. *Adv. Water Resour.* **141**, 103615 (2020)
- Wang, X., Pan, J., Wang, K., Ge, T., Wei, J., Wu, W.: Characterizing the shape, size, and distribution heterogeneity of pore-fractures in high rank coal based on X-ray CT image analysis and mercury intrusion porosimetry. *Fuel* **282**, 118754 (2020)
- Washburn, E.W.: The dynamics of capillary flow. *Phys. Rev.* **17**, 273–283 (1921)
- Wiegmann, A.J.B.: Virtual characterization of the pore structure of nonwoven. In: International Nonwoven Technical Conference, Atlanta. Atlanta (2007)
- Wu, H., Schwartz, D.K.: Nano-particle tracking to probe transport in porous media. *Acc. Chem. Res.* **53**, 2148–2156 (2020)
- Wu, J., Yuan, Y., Niu, S., Wei, X., Yang, J.: Multiscale characterization of pore structure and connectivity of Wufeng–Longmaxi shale in Sichuan Basin, China. *Mar. Pet. Geol.* **120**, 104514 (2020)
- Zhang, L., Kou, Z., Wang, H., Zhao, Y., Dejam, M., Guo, J., Du, J.: Performance analysis for a model of a multi-wing hydraulically fractured vertical well in a coalbed methane gas reservoir. *J. Pet. Sci. Eng.* **166**, 104–120 (2018)

- Zhang, P., Lu, S., Li, J.: Characterization of pore size distributions of shale oil reservoirs: a case study from Dongying sag, Bohai Bay basin, China. *Mar. Pet. Geol.* **100**, 297–308 (2019)
- Zhao, Y., Sun, Y., Liu, S., Wang, K., Jiang, Y.: Pore structure characterization of coal by NMR cryoporometry. *Fuel* **190**, 359–369 (2017)
- Zhao, Y., Peng, L., Liu, S., Cao, B., Sun, Y., Hou, B.: Pore structure characterization of shales using synchrotron SAXS and NMR cryoporometry. *Mar. Pet. Geol.* **102**, 116–125 (2019)

Publisher's Note Springer Nature remains neutral with regard to jurisdictional claims in published maps and institutional affiliations.

Affiliations

Mehdi Razavifar¹ · Aliya Mukhametdinova² · Ehsan Nikooee¹ · Alexander Burukhin² · Amin Rezaei¹ · Alexey Cheremisin² · Masoud Riazi¹ 

✉ Masoud Riazi
mriazi@shirazu.ac.ir

Alexey Cheremisin
a.cheremisin@skoltech.ru

¹ Enhanced Oil Recovery (EOR) Research Centre, IOR/EOR Research Institute, Shiraz University, Shiraz, Iran

² Center for Hydrocarbon Recovery, Skolkovo Institute of Science and Technology, Moscow, Russia